Nuclear Instruments and Methods in Physics Research A 664 (2012) 111–116

Contents lists available at SciVerse ScienceDirect

Nuclear Instruments and Methods in Physics Research A

journal homepage: www.elsevier.com/locate/nima

A correction to Birks' Law in liquid argon ionization chamber simulations for highly ionizing particles

Sergey Burdin [a], Marko Horbatsch [b], Wendy Taylor [b,*]

[a] Department of Physics, University of Liverpool, Liverpool L69 7ZE, UK
[b] Department of Physics and Astronomy, York University, Toronto, ON, Canada M3J 1P3

ARTICLE INFO

Article history:
Received 19 May 2011
Received in revised form
6 October 2011
Accepted 31 October 2011
Available online 7 November 2011

Keywords:
Highly ionizing particle
Birks' Law
Liquid argon calorimeter
Ionization
Recombination
Simulation

ABSTRACT

We present a study of the performance of Birks' Law in liquid argon ionization chamber simulations as applied to highly ionizing particles, such as particles with multiple electric charges or with magnetic charge. We used Birks' Law to model recombination effects in a GEANT4 simulation of heavy ions in a liquid argon calorimeter. We then compared the simulation to published heavy-ion data to extract a highly ionizing particle correction to Birks' Law.

1. Introduction

Searches for exotic highly ionizing particles, such as Q-balls [1] and magnetic monopoles, are underway at the Large Hadron Collider (LHC) at the CERN laboratory in Geneva, Switzerland. A Q-ball [2] is an exotic particle with an electric charge greater than the elementary charge unit $|e|$. Q-balls, having multiple electric charges $|q|=z|e|$, where z is some integer, are highly ionizing compared to singly charged particles, since the energy deposited per unit length is proportional to z^2 [3]. The basic magnetic monopole [4] is electrically neutral but has a "magnetic charge", g. Magnetic monopoles are also highly ionizing, interacting with matter in a manner similar to that of an ion of $z=68.5$ [4]. We refer to such particles as highly ionizing particles, or HIPs. In order to search for such hypothetical particles, it is necessary to understand how they would appear in the detector.

At the ATLAS Experiment [5], the characteristic signature of such HIPs includes a large localized energy deposit in the liquid argon (LAr) electromagnetic (EM) calorimeter and the production of a large number of δ-rays, which are energetic "knock-on" electrons emitted perpendicularly to the trajectory of the HIP. The narrow energetic shower in the LAr calorimeter would be a striking signature but for recombination effects. When an ionizing particle passes through the liquid argon, it loses energy via its Coulomb interactions with the argon nuclei and electrons (see Ref. [6] for a comprehensive review of stopping power). The total energy deposition is due to ionization and electronic excitations; the latter give rise to scintillation, which is not recorded by ATLAS. The energy lost due to interactions with the nuclei, which lead to phonon excitations, can be neglected except at very low projectile velocities.

In addition to δ-rays, soft electrons are produced by the interactions with the argon atoms, resulting in electron-ion pairs in the region of high ionization density, called the *core*, around the HIP trajectory. The δ-rays carry energy away from the core, go on to ionize the medium themselves and give rise to a region of lower ionization density, called the *penumbra*, which surrounds the core [7].

In a LAr calorimeter, an electric field is applied to collect the ionized electrons. The charge collected is then scaled appropriately to deduce the total amount of deposited energy. However, some electron–ion pairs may recombine before the ionization electron can be recorded, particularly in the core. This recombination effect reduces the recorded charge and, consequently, the deposited energy is underestimated. The recombination effect is inversely proportional to the electric field. A higher electric field accelerates the ionization electrons away from the ions more quickly, before they can recombine. Conversely, the recombination effect is proportional to the ionization density, that is, the energy deposited per unit length, dE/dx. When more ions are

* Corresponding author. Tel.: +1 416 736 2100x77758; fax: +1 416 736 5516.
E-mail address: taylorw@yorku.ca (W. Taylor).

0168-9002/$ - see front matter © 2011 Elsevier B.V. All rights reserved.
doi:10.1016/j.nima.2011.10.044

available nearby, the electrons will be more likely to recombine with them. These two relationships can be described by the function

$$Q = Q_0 \frac{A}{1+\frac{k}{\rho E_D}\frac{dE}{dx}} \quad (1)$$

where Q_0 is the charge produced, Q is the recorded charge, E_D is the drift electric field, ρ is the density of the liquid argon, and A and k are the parameters that must be extracted from a fit to data. The so-called *recombination factor* $R = Q/Q_0$ reflects the fraction of charge that is "visible". Eq. (1) is commonly referred to as Birks' Law [8], which was originally developed to describe the response of organic scintillators to ionizing particles. The ICARUS collaboration showed that Eq. (1) describes the ionization response of their LAr Time Projection Chamber to cosmic-ray muons and protons [9]. ICARUS measured the parameter k, commonly referred to as Birks' constant, to be

$$k = 0.0486 \pm 0.0006\ (\mathrm{kV/cm})((\mathrm{g/cm^2})/\mathrm{MeV}) \quad (2)$$

valid in the drift electric field range $0.1 < E_D < 1.0$ kV/cm and in the ionization density range $2.1 < dE/dx < 42$ MeV/cm. The normalization parameter measured by ICARUS is $A = 0.800 \pm 0.003$.

The present study establishes that Birks' Law with a single set of Birks' constant and normalization parameter cannot accurately describe the behavior of ionizing particles in liquid argon simulations over a large dE/dx range. In particular, while the ICARUS measurements of Birks' constant and normalization parameter are appropriate for singly charged particles, as expected, Birks' Law overestimates the recombination effects for particles with large dE/dx.

For our study, we used a GEANT4 [10] simulation of ions interacting in a LAr detector and modelled recombination effects using Birks' Law with values of Birks' constant and normalization parameter as measured by ICARUS. We then compared the simulation to published data of heavy ions interacting in a 2-cm liquid argon detector [11–13] and extracted a highly ionizing particle correction to Birks' Law. This technique should be applicable to other liquid argon and liquid xenon detectors [14], which are commonly used to measure the presence of subatomic particles via ionization, and to other simulation platforms.

2. LAr GEANT4 simulation

The GEANT4 simulation package contains many classes that model the energy deposition of particles passing through matter. The present study relies on a subset of electromagnetic interaction models [15]. Highly energetic ions that pass through a finite amount of LAr deposit only a small fraction of their initial energy. In this regime, the description of energy loss of the highly ionizing particle by the Bethe–Bloch formula is considered to be accurate to better than 1% [16].

In the GEANT4 simulation, the G4ionIonisation class [15], which models both electronic and nuclear stopping power effects, was used to simulate the continuous energy loss of the heavy ion[1] and the production of δ-rays, as described in Ref. [16]. The latter process is modelled by the scattering of the projectile from quasi-free electrons. For a given projectile kinetic energy, the resulting δ-rays can have energy T up to a maximum value $T_{\max} \approx 2m_e c^2(\gamma^2-1)$, where m_e is the electron mass and γ is the Lorentz factor of the projectile. In order to conserve computational resources, GEANT4 does not propagate low-energy δ-rays, i.e., electrons with energy below a minimum threshold T_{cut} are not simulated explicitly. In this case, the corresponding energy loss is added to the energy loss of the ion continuously during the discrete "step" in the trajectory propagation. For convenience, T_{cut} is controlled in GEANT4 by the related *cut in range* [10] parameter. In the present study, the range cut was set to 100 μm, the default value used in the ATLAS LAr EM calorimeter simulation. For our purposes, this parameter effectively dictates the fraction of energy explicitly deposited by δ-rays relative to that deposited by the primary ion. The energy deposition of the transported δ-rays with $T_{\mathrm{cut}} < T < T_{\max}$ is modelled with the G4eIonisation class, which includes secondary δ-ray and Bremsstrahlung production.

The GEANT4 simulation of energy deposition has been validated for both ions and δ-rays. In Fig. 8 of Ref. [10], the stopping power due to ionization losses in Al is shown to agree with data for C and Ar projectiles over a large energy range. For proton and alpha particle impact, GEANT4 has been validated against NIST reference data [17]. The simulation of δ-ray production and propagation due to 2–50 GeV electrons passing through silicon wafers has also been tested [18].

In the present simulation of each heavy-ion experiment, the kinetic energy of the simulated ion is set to the heavy-ion beam energy. The ion is then transported through the 2-cm detector in a series of steps of length Δx. In each step, ΔE_0 is the true energy deposited via ionization. The visible step energy deposition ΔE_{vis} is then obtained by correcting ΔE_0 using Birks' Law

$$\Delta E_{vis} = \Delta E_0 \frac{A}{1+\frac{k}{\rho E_D}\frac{dE}{dx}} \quad (3)$$

where E_D has a value between 1 kV/cm and 10 kV/cm, dE/dx is taken as $\Delta E_0/\Delta x$ for each step, $k = 0.0486$ (kV/cm)((g/cm^2)/MeV) and $A = 0.800$, as measured by ICARUS. Then, the total true and visible energies are determined by summing the true and visible step energies, respectively, for all steps. The ratio of visible to true energies yields the recombination factor $R_{MC} = E_{vis}/E_0$ that we can compare directly to the heavy-ion experimental ionization data due to the fact that the charge produced, Q_0, is proportional to the energy deposited, E_0 [7].

3. Performance of Birks'-Law-corrected GEANT4 simulation for heavy ions in LAr

In the heavy-ion experimental papers [11–13], the experimenters measured the ionization current fraction $R_{Exp} = I/I_\infty$, where I is the recorded current and I_∞ is the expected ionization current assuming a drift electric field of infinite strength. In the present study, we compare the recombination factor $R_{MC} = E_{vis}/E_0$ to the measured factor $R_{Exp} = I/I_\infty$. The properties of the experimental data are given in Table 1.

Fig. 1 shows the comparison of the GEANT4 simulation to the experimental data for each heavy ion. The measured ionization current fractions were extracted from the plots in the published papers [11–13]; they are shown as a function of drift electric field (triangles). The error bars reflect the 14% uncertainty in I/I_∞, where 13% is due to the uncertainty in the expected values of I_∞ and 1% is due to the measured ionization currents I [12]. The data curves can be compared to the simulation curves (circles), which give the visible energy fraction as a function of drift electric field, as observed in the simulation. The curves themselves represent not fits but spline interpolations between the points.

One expects that Birks' Law with $k = 0.0486$ (kV/cm) ((g/cm^2)/MeV) and $A = 0.800$, as measured by ICARUS, should agree with the proton experimental data. Indeed, this is the case for hydrogen, helium and even neon, as can be seen in Fig. 1a–c. However,

[1] Proton energy loss was modelled with the G4hIonisation class, which neglects nuclear effects.

Table 1
Properties for each heavy-ion beam [11–13,19] in the 2-cm liquid argon detector. The bottom row gives the average dE/dx values of the primary ion in the simulation for a range cut of 100 μm; these are provided for comparison with the predicted dE/dx values given in Refs. [11–13,19].

Ion property	H	He	Ne	Fe	La	Au
Charge ($\|e\|$)	1	2	10	26	57	79
Mass (GeV/c^2)	0.93885	3.7284	18.797	52.019	129.390	183.473
Kinetic energy (GeV)	1.048	4.1627	12.370	39.371	169.46	171.36
dE/dx (MeV/cm)	2.235	8.95	259.26	1655	7750	16 200
dE/dx (MeV/cm) (our simulation)	1.895	7.42	223.28	1470	6218	13 141

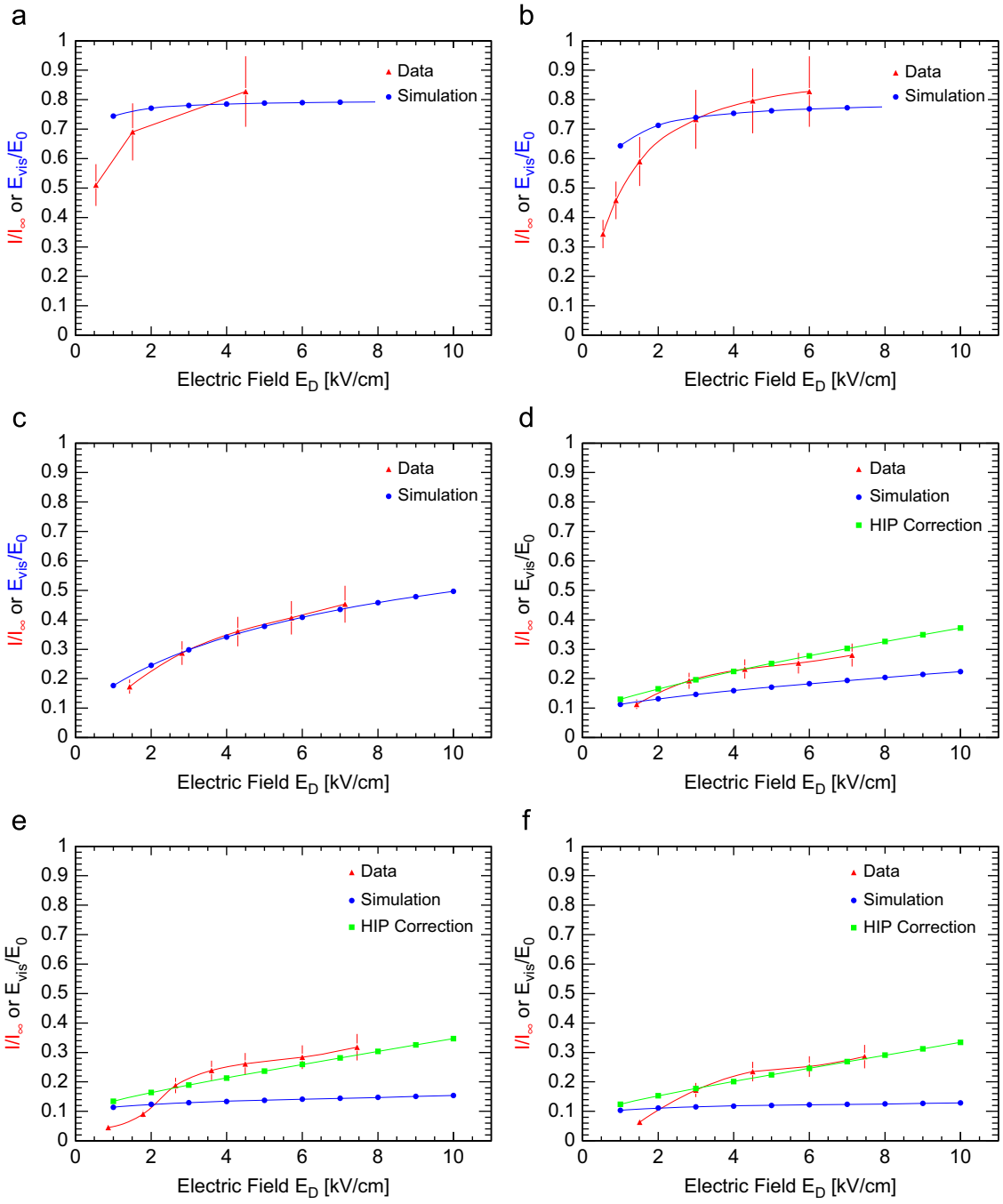

Fig. 1. Recombination factor R as a function of drift electric field E_D for various heavy ions in liquid argon. The triangles are the experimental ionization fractions [11–13]. The circles are the simulated visible energy fractions. The squares are the simulated visible energy fractions after the application of the HIP correction, described herein. (a) H ions, (b) He ions, (c) Ne ions, (d) Fe ions, (e) La ions and (f) Au ions.

the simulation with Birks' Law disagrees with the experimental data for the more highly charged ions. For low drift fields, the La and Au experimental data show some space-charge effects [11], which are not modelled in the GEANT4 simulation. For high drift fields, the disagreement appears to be due to an over-suppression by Birks' Law, as can be seen in Fig. 2, which shows the ionization

current fraction I/I_∞ as a function of dE/dx for the various heavy ions for $E_D=7$ kV/cm. In the figure, the points, from left to right, reflect each heavy-ion experiment. Overlaid is Birks' Law with $k=0.0486$ (kV/cm)((g/cm^2)/MeV) and $A=0.800$, as measured by ICARUS.

It is unreasonable to expect Birks' Law to apply over a large dE/dx range, since it is only a first-order expansion of $1/R$ in dE/dx. Unfortunately, a simple extension of Birks' Law to higher order in dE/dx cannot account for the fact that the ionization current fraction becomes independent of dE/dx above 1000 MeV/cm. Another reason why it is unreasonable to expect Birks' Law to describe the high-dE/dx data in Fig. 2 is that the energy deposition of δ-rays has not been properly taken into account. The number of δ-rays produced is proportional to the dE/dx of the ionizing projectile. However, since δ-rays themselves have low ionization density, the energy carried away from the core by the δ-rays is not suppressed by recombination effects. Therefore, it is necessary to make an assumption about the fraction of energy deposited by the primary ion. This can be obtained from the GEANT4 simulation for a given range cut, as illustrated in Fig. 3, which shows the visible energy fraction $R_{MC}=E_{vis}/E_0$ as a function of dE/dx for the various heavy ions for $E_D=7$ kV/cm. In the figure, the points, from left to right, reflect a simulation of each heavy-ion experiment. The various curves reflect range cuts from 1 μm to 1000 μm. As can be seen in the figure, the high-dE/dx primary ions contribute very little to the visible energy. Indeed, using a range cut of 100 μm, at $E_D=7$ kV/cm δ-rays account for 15% of the total energy deposited by gold ions but 92% of the visible energy. This explains the independence of the ionization current fraction on dE/dx above 1000 MeV/cm. Furthermore, in the simulation, at high dE/dx the total visible energy depends strongly on the range cut, which controls the fraction of energy deposited by the δ-rays.

4. HIP correction to Birks' Law in liquid argon

We have shown that an implementation of Birks' Law with the ICARUS values of Birks' constant and normalization parameter in a LAr GEANT4 simulation underestimates the visible energy for ions with $z \geq 26$ for $E_D > 3$ kV/cm. As the behavior of such a simulation for muons, electrons and pions at $E_D=10$ kV/cm has been verified elsewhere [20–22], our main concern is the high-dE/dx region, populated by magnetic monopoles and high-charge Q-balls.

A comparison of the simulation and the heavy-ion data over the range of dE/dx represented in the data can be seen in Fig. 4. In the figure, the y-axis shows the ratio R_{MC}/R_{Exp} for $E_D=7$ kV/cm. The data points, from left to right, reflect each heavy-ion experiment. The error bars reflect the 14% uncertainty in $R_{Exp}=I/I_\infty$

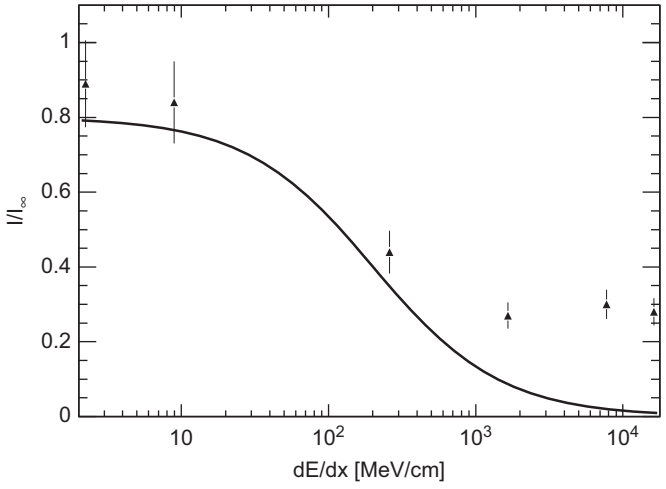

Fig. 2. Experimental ionization current fraction I/I_∞ [11–13] as a function of dE/dx for various heavy ions for $E_D=7$ kV/cm in liquid argon. The values of I/I_∞ are extrapolated from the curves in Fig. 1. Overlaid is Birks' Law with $k=0.0486$ (kV/cm)((g/cm^2)/MeV) and $A=0.800$.

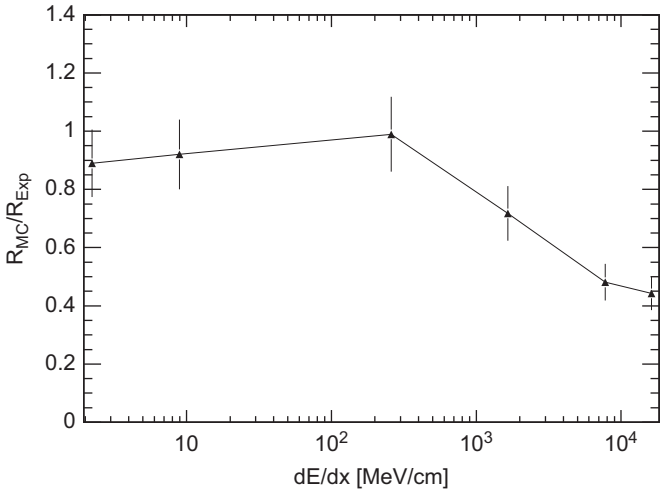

Fig. 4. The performance R_{MC}/R_{Exp} of the GEANT4 simulation including Birks' Law as a function of dE/dx for various heavy ions for $E_D=7$ kV/cm and a range cut of 100 μm.

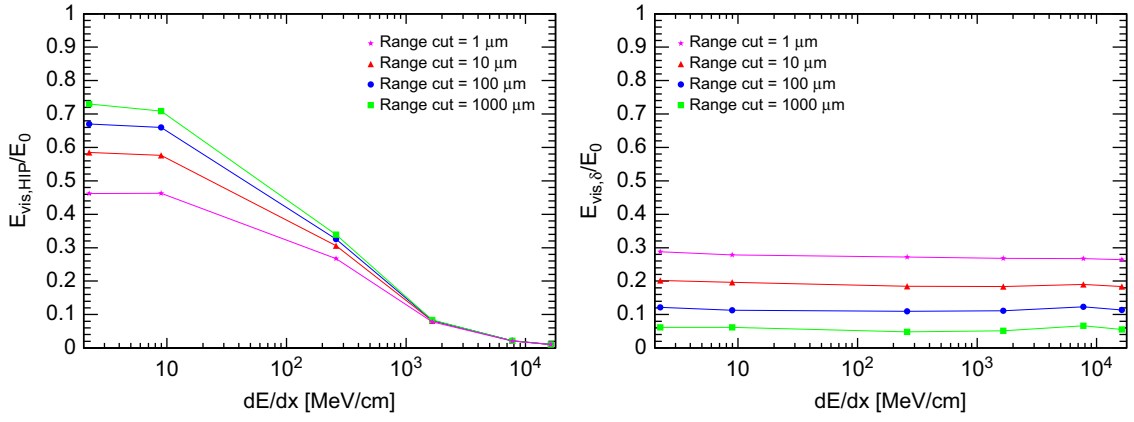

Fig. 3. The visible energy fraction $R_{MC}=E_{vis}/E_0$ as a function of dE/dx for various heavy ions for $E_D=7$ kV/cm. E_0 is the *total* energy deposited by both the ion and the δ-rays. The plot on the left represents the visible energy deposited by the primary ion. The plot on the right represents the visible energy deposited by the δ-rays. The various curves reflect range cuts from 1 μm to 1000 μm. The x-axis uses the predicted dE/dx values, since the dE/dx values in the simulation depend on the range cut.

[12]. As can be seen in the figure, the simulation gives a reasonable description of the visible energy in the low-dE/dx region, as expected. In particular, the ratio R_{MC}/R_{Exp} is consistent with unity within uncertainties for both hydrogen, helium and neon ions. However, the simulation significantly underestimates the visible energy at high dE/dx. This discrepancy can be parametrized to obtain a HIP visible energy correction to Birks' Law, to extend its dE/dx validity range.

Unfortunately, one cannot simply use a parametrization of the curve shown in Fig. 4 to correct the visible step energy in the simulation. This is because a significant fraction of the visible energy associated with HIPs is deposited by δ-rays, as shown in Figs. 3 and 5.

In the simulation, the sum of the visible energies of the primary ion and the δ-rays yields the total visible energy, that is,

$$R_{MC} = \frac{E_{vis}}{E_0} = \frac{E_{vis,HIP} + E_{vis,\delta}}{E_0}. \quad (4)$$

Thus, the left and right plots of Fig. 5 combine to yield Fig. 4. Having separated out the component due to the primary ion only, we can parametrize the plot on the left in Fig. 5 to obtain the desired HIP correction that yields $R_{MC}/R_{Exp} = 1$, that is,

$$\frac{R_{MC}}{R_{Exp}} = \frac{C_{HIP}E_{vis,HIP} + C_\delta E_{vis,\delta}}{E_0}\frac{1}{R_{Exp}} = 1 \quad (5)$$

where C_{HIP} and C_δ are the correction factors for the HIP and δ-rays, respectively. However, $C_\delta \approx 1$ since the dE/dx of the δ-rays is very low. This yields

$$C_{HIP} = \frac{R_{Exp}E_0 - E_{vis,\delta}}{E_{vis,HIP}}. \quad (6)$$

C_{HIP} was calculated for each of the ions at $E_D = 7$ kV/cm. Its dependence on dE/dx is shown in Fig. 6. In the figure, the dE/dx values are taken from the simulation and reflect the energy deposited by the primary ion only. The error bars reflect the 14% uncertainty in R_{Exp}. A linear fit to the data for the Ne, Fe, La and Au ions yields the y-intercept $p_0 = 0.715 \pm 0.184$ and slope $p_1 = 0.00109 \pm 0.00018$ cm/MeV, such that the HIP correction is

$$C_{HIP} = \begin{cases} 1, & dE/dx \le 262 \\ 0.00109\dfrac{dE}{dx} + 0.715, & dE/dx > 262 \end{cases} \quad (7)$$

where dE/dx is given in MeV/cm. The lower dE/dx bound for the HIP correction is obtained by setting $C_{HIP} = 1$; no correction is applied for lower values of dE/dx, since this regime has been verified elsewhere [20–22].

We emphasize that this correction is only applicable for a range cut of 100 μm. If a different range cut is used, then the present study must be repeated to obtain the appropriate HIP correction. As an example, the dependence of the performance of Birks' Law in the GEANT4 LAr simulation on the range cut is shown in Fig. 7. The reduction of the range cut from 100 μm to 10 μm results in the production of more δ-rays. The fraction of energy deposited by the δ-rays increases (see Fig. 3), mitigating somewhat the recombination effects for highly ionizing particles.

5. Performance of HIP correction to Birks' Law in liquid argon

As discussed earlier, the true energy deposited by a particle via ionization is available in each step of the trajectory propagation in the simulation. The step energy deposition is first corrected using Birks' Law. Subsequently, the HIP correction in Eq. (7) is applied to the Birks'-corrected step energy to determine the visible step energy deposition, i.e.,

$$E_{vis} = C_{HIP}\left(\frac{AE_0}{1 + \dfrac{k}{\rho E_D}\dfrac{dE}{dx}}\right)$$

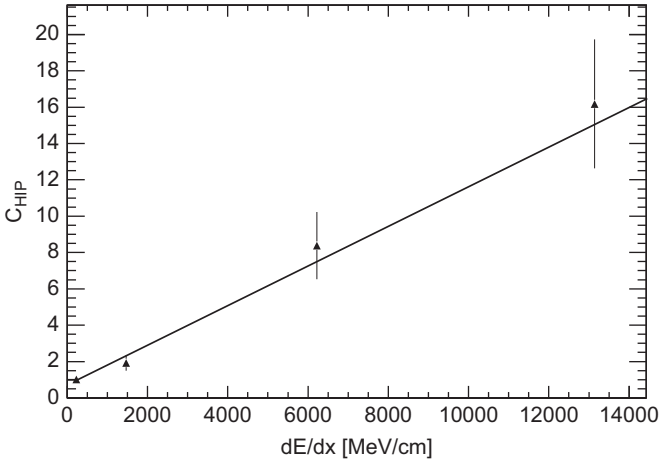

Fig. 6. HIP correction factor C_{HIP} as a function of dE/dx for Ne, Fe, La and Au ions for $E_D = 7$ kV/cm. The dE/dx values are taken from the simulation and reflect the energy deposited by the primary ion only. The H and He ion points are not shown.

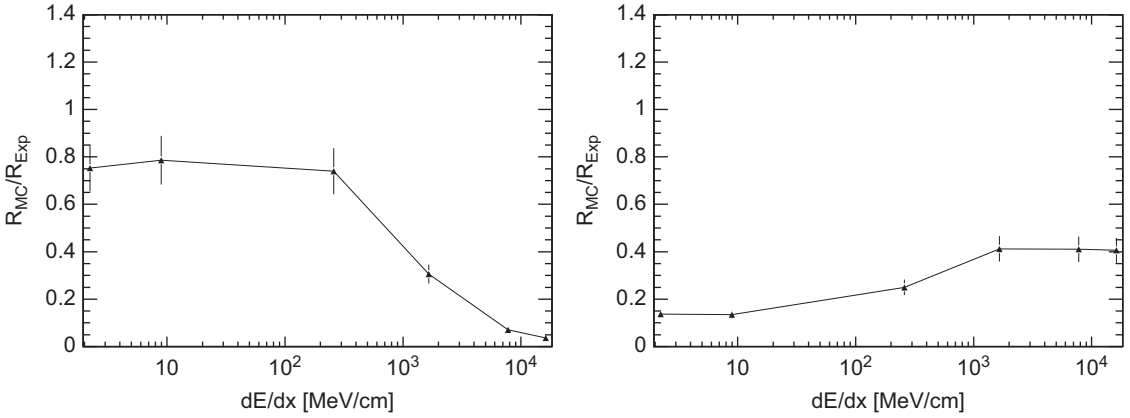

Fig. 5. The performance R_{MC}/R_{Exp} of Birks' Law as a function of dE/dx for various heavy ions for $E_D = 7$ kV/cm and a range cut of 100 μm. The plot on the left represents the visible energy deposited by the primary ion. The plot on the right represents the visible energy deposited by the δ-rays.

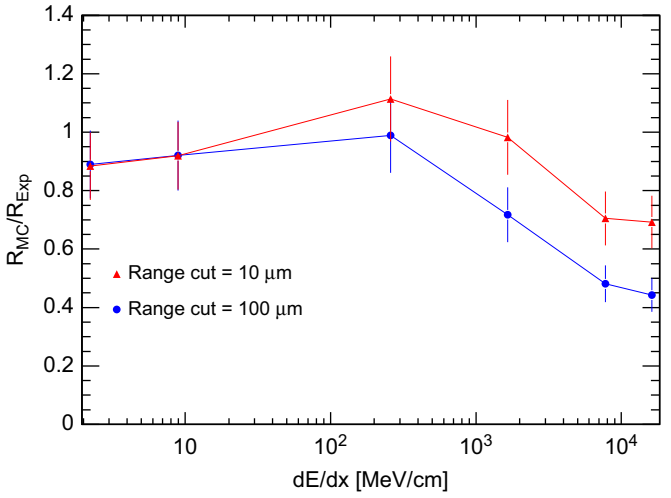

Fig. 7. The performance R_{MC}/R_{Exp} of the GEANT4 simulation with Birks' Law as a function of dE/dx for various heavy ions for E_D=7 kV/cm. The circles are for a range cut of 100 μm, whereas the triangles are for a range cut of 10 μm.

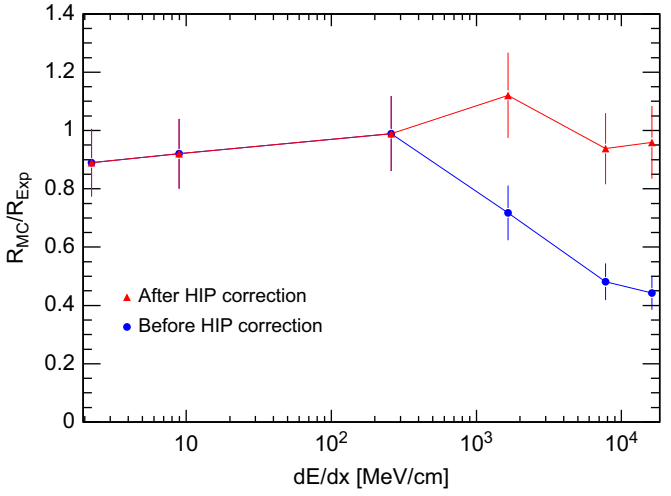

Fig. 8. The performance R_{MC}/R_{Exp} of the GEANT4 simulation including Birks' Law as a function of dE/dx for various heavy ions for E_D=7 kV/cm and a range cut of 100 μm. The triangles show the performance after the application of the HIP correction. The circles reflect the performance prior to the application of the HIP correction for comparison.

$$= \left(0.00109\frac{dE}{dx} + 0.715\right)\frac{AE_0}{1+\frac{k}{\rho E_D}\frac{dE}{dx}} \quad (8)$$

for particles with $dE/dx > 262$ MeV/cm in that step. Although the HIP correction in Eq. (7) was obtained for a drift field E_D=7 kV/cm, the HIP-corrected form of Birks' Law in Eq. (8) improves the simulation of the recombination effects over a broad range of drift fields, as demonstrated in Fig. 1d–f. The resulting improvement in the performance of the GEANT4 LAr simulation is shown in Fig. 8. As can be seen in the figure, the agreement between the simulation and the heavy-ion data is significantly better at high dE/dx, while the performance remains unchanged for low-dE/dx particles, such as electrons, pions and muons, as required.

6. Conclusion

We have shown that a GEANT4 LAr simulation including Birks' Law to model recombination effects underestimates the visible energy for highly ionizing particles at high drift electric fields. We developed a method to extend the validity range of Birks' Law to high dE/dx, in which we compared the results of a GEANT4 simulation of heavy-ion interactions in liquid argon, including Birks' Law with the ICARUS measurements of Birks' constant and normalization parameter, to published heavy-ion data and extracted a highly ionizing particle correction to Birks' Law. This HIP correction improves the performance of the simulation for highly ionizing particles.

Acknowledgements

S. Burdin and W. Taylor would like to thank Vladimir Ivanchenko for helpful discussions. The authors acknowledge support from the Science and Technology Facilities Council, United Kingdom, and from NSERC and the Canada Research Chair program, Canada.

References

[1] B. Aad, et al., Physics Letters B 698 (2011) 353.
[2] S. Coleman, Nuclear Physics B 262 (1985) 263.
[3] H. Bethe, Annals of Physics (Leipzig) 5 (1930) 325;
F. Bloch, Annals of Physics (Leipzig) 16 (1933) 285.
[4] P.A.M. Dirac, Proceedings of the Royal Society A 133 (1931) 60.
[5] G. Aad, et al., Journal of Instrumentation 3 (2008) S08003.
[6] C. Leroy, P.-G. Rancoita, Principles of Radiation Interaction in Matter and Detection, World Scientific Publishing, 2009.
[7] A. Hitachi, T. Doke, A. Mozumder, Physical Review B 46 (1992) 11463.
[8] J.B. Birks, Proceedings of the Physical Society A 64 (1951) 874;
J.B. Birks, Proceedings of the Physical Society A 64 (1951) 511;
J.B. Birks, Theory and Practice of Scintillation Counting, Pergamon Press, 1964.
[9] S. Amoruso, et al., Nuclear Instruments and Methods in Physics Research Section A 523 (2004) 275.
[10] S. Agostinelli, et al., Nuclear Instruments and Methods in Physics Research Section A 506 (2003) 250.
[11] E. Shibamura, et al., Nuclear Instruments and Methods in Physics Research Section A 260 (1987) 437.
[12] T. Doke, et al., Nuclear Instruments and Methods in Physics Research Section A 235 (1985) 136.
[13] H.J. Crawford, et al., Nuclear Instruments and Methods in Physics Research Section A 256 (1987) 47.
[14] E. Aprile, et al., Nuclear Instruments and Methods in Physics Research Section A 307 (1991) 119 and references therein.
[15] 〈http://geant4.cern.ch/collaboration/working_groups/electromagnetic/index.shtml〉, 〈http://geant4.web.cern.ch/geant4/UserDocumentation/UsersGuides/PhysicsReferenceManual/fo/PhysicsReferenceManual.pdf〉.
[16] A. Bagulya, et al., Bulletin of the Lebedev Physics Institute 36 (2009) 29.
[17] K. Amako, et al., IEEE Transactions on Nuclear Science NS-52 (2005) 910.
[18] S.R. Hou, et al., Nuclear Instruments and Methods in Physics Research Section A 418 (1998) 145.
[19] T. Doke, et al., Nuclear Instruments and Methods in Physics Research Section A 269 (1988) 291.
[20] M. Aharrouche, et al., Nuclear Instruments and Methods in Physics Research Section A 606 (2009) 419.
[21] M. Aharrouche, et al., Nuclear Instruments and Methods in Physics Research Section A 614 (2010) 400.
[22] E. Abat, et al., ATL-CAL-PUB-2010-001, ATLAS Technical Note.